INFLUENCE OF THE NUMBER OF VORTEX ELEMENTS ON THE STABILITY AND ACCURACY OF THE NUMERICAL SIMULATION FOR A ROTOR IN HOVER

Filip PANAYOTOV[*], Ivan DOBREV[**], Fawaz MASSOUH[**], Michael TODOROV*

[*]Technical University of Sofia, Bulgaria (michael.todorov@tu-sofia.bg)
[**]Arts et Métiers - ParisTech, Paris, France (fawaz.massouh@ensam.eu)

DOI: 10.19062/1842-9238.2017.15.3.3

Abstract: *Numerical simulations based on vortex models are very sensible from both the number of vortex elements and the initial conditions. The aim of this study is to evaluate the influence of the number of the vortex elements, modelling the wake, on the stability and accuracy of the numerical solution for the performance of a rotor in hover. For each computational case the number of the vortex elements varies from the number of blades per rotor and from the number of the emitted vortices per blade, which are taken into account. It was observed that larger series of vortex rings provide more accurate results, while a quicker convergence of the numerical solution is achieved with a smaller number of vortex elements. The use of time-stepping predictor-corrector scheme of second order, contributed for an increased stability of the simulation of the convection and propagation of the free-wake in the computational domain. The numerical results are compared against previously obtained experimental data for a model rotor.*

Keywords: *rotor; hover; rotor wake; flow-field; induced velocity; vortex ring; vortex cylinder;*

1. INTRODUCTION AND STATE OF THE ART

Unmanned air vehicles (UAVs) have recently become increasingly popular amongst civilians, scientists and the military. Regardless of their size and utility, those are mainly divided into two major groups: fixed-wing and rotary-wing vehicles. The main difference between the two types of air vehicles is the way they produce lift and their aims of directional control.

The main advantage of the rotary wing UAVs is the possibility to perform hover. Widespread are the multi-rotor flying platforms, especially the multicopter (one of which is the quadcopter), which have one rotor at each corner. This configuration became very popular due to the possibility to achieve easy balance and control of the flying platform.

Whatever the purpose of a rotary wing UAV, whether it is a main-rotor/tail-rotor configuration or it is a multi-rotor configuration, there are two possible approaches for the control of their propulsion systems: to vary the rotational speed of a rotor with a fixed geometry or to change the pitch angle of the blades of the rotor, which operates at a constant rotational speed. Both control approaches produce the same result, as any increase in the rotational speed of the rotor or the pitch angle of the blades increases the produced thrust, while any decrease in both control inputs decreases it.

Regardless of the applied control method for the thrust production of all major rotary-wing based UAVs, their rotors operate in unsteady conditions due to the fact they are rarely performing long lasting hovers in zero wind conditions.

The typical flight utility of the rotary-wing vehicles is such that they are constantly maneuvering or performing thrust adjustments, in order to maintain stable flight or hover, while compensating for atmospheric disturbances. Thus of great interest is the rotor performance during transient and unsteady operating regimes, which are produced by rapid changes in the rotational speed of the rotor or by significant sudden changes of the pitch angle of the blades of the rotor.

As shown by Leishman in [1], the blade element momentum theory allows for the rapid computation of the forces acting on the blades of a rotor, thus allowing for the rapid evaluation of the overall rotor performance. However, in order for a BEM model to provide accurate estimations, the exact radial distribution of the induced speed must be known and the appropriate tip-loss corrections must be applied.

As shown in [2, 3, 4 and 5], the application of the vortex theory allows for the computations of the induced velocity field in all the computational domain around the rotor, including for the plane of the rotor. This provides accurate data for the radial distribution of the induced velocity, which is then used by the BEM model.

In [6, 7 and 8], demonstrated is the ability of the vortex models to compute the exact geometry of the rotor wake. In [9 and 10], shown are the positive effects from the use of predictor-corrector algorithms on the stability and accuracy of the numerical solutions for the wake geometry of rotors in hover.

Thus, by coupling a BEM model with a vortex model and with the introduction of a time-step marching algorithm, it is possible to obtain a valuable numerical tool, which allows the possibility to study the rotor performance in unsteady flow conditions, resulting from the transition from one operating regime to another or from phenomenons, such as the tip vortex aperiodicity of a hovering rotor [11]. In [12] is shown the capability of such a coupled BEM-vortex numerical model to adequately predict the airload of the blades of the rotor both in hover and in forward flight.

2. NUMERICAL MODEL

Modelling the wake of a hovering rotor with a combination of different types of vortex elements for different segments of the wake is demonstrated in [2-12]. The comparison study is performed with the vortex model proposed by Miller et al. in [12]. In the remainder part of the article it will be referred as the Miller model.

The wake of the Miller model consists of two parts: a near wake composed of 20 circular vortex rings arranged in series downstream of the rotor; and a far wake modelled by a single semi-infinite vortex cylinder, placed behind the last vortex ring of the near wake. Thus the model consists of only 21 vortex elements to be accounted for the computation of the entire flow-field around the rotor.

The semi-infinite vortex cylinder allows the model to compensate for the velocity deficit formed downstream of a wake when modelled with a series of vortex rings. It allows to stabilize the numerical computation and ensures that the induced velocities in the far wake double those induced in the rotor plane, such as per the theory for the hovering rotor.

Key for the degree of accuracy and the adequate operation of the model is the proper setup of the parameters d_0 and d_1, shown on Fig. 1.

The distance d_0, at which the first vortex ring is placed behind the rotor, has a key role for the distribution of the induced velocities along the blade. It is referred in [12] as the first blade-vortex encounter position, which represents the distance between the vortex ring emitted by the preceding blade and the following blade.

This parameter can be varied, in order to study its influence on the induced velocity distribution on the blades and in the near wake downstream of the rotor.

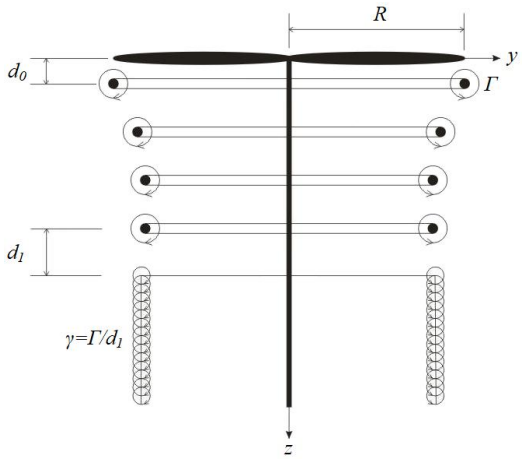

FIG. 1. T Schematic representation of the arrangement of the vortex elements for the Miller model.

The distance d_1 is the spacing between the last vortex ring of the near wake and the semi-infinite vortex cylinder, which models the far wake. The optimal values of the parameters d_0 and d_1 are estimated in a comparison between numerical and experimental data for multiple operational regimes of the rotor.

The Miller model offers the potential for rapid computation of the velocity flow-field around a rotor, when compared to CFD models, due to the necessity to perform significantly smaller amount of computations by solving only few thousand simple elliptical integrals, instead of few hundred thousand Navier-Stokes equations. An additional reduction of the volume of numerical computations is possible for hover and vertical flight regimes due to the presence of axis-symmetric flow condition for the rotor.

3. NUMERICAL STUDIES

The performed numerical study aims to evaluate the stability and accuracy of the free wake model with regards to the different number vortex rings, used to .

Computed are the mutually induced and the self-induced velocities between the vortex elements modelling the wake. The induced velocities on each vortex element are then used to compute its new position in the wake for the next computational time step Δt. Thus, the vortex rings propagate in the numerical domain and take the necessary geometry arrangement, in order to adapt to the latest flow conditions.

Once the solution has converged and the equilibrium arrangement of the vortex elements is obtained, then the distribution of the induced velocity V_z along the blades is computed. Thus, by knowing the angular velocity of the rotor Ω and the pitch angle of the blades θ, it is possible to determine the aerodynamic forces acting on the blades. Those forces are used for the computation of the net trust T produced by the rotor and the required mechanical power P for the rotor to perform hover. This computational cycle repeats itself for each time step Δt of the simulated time-period. The described algorithm is shown on Fig. 2.

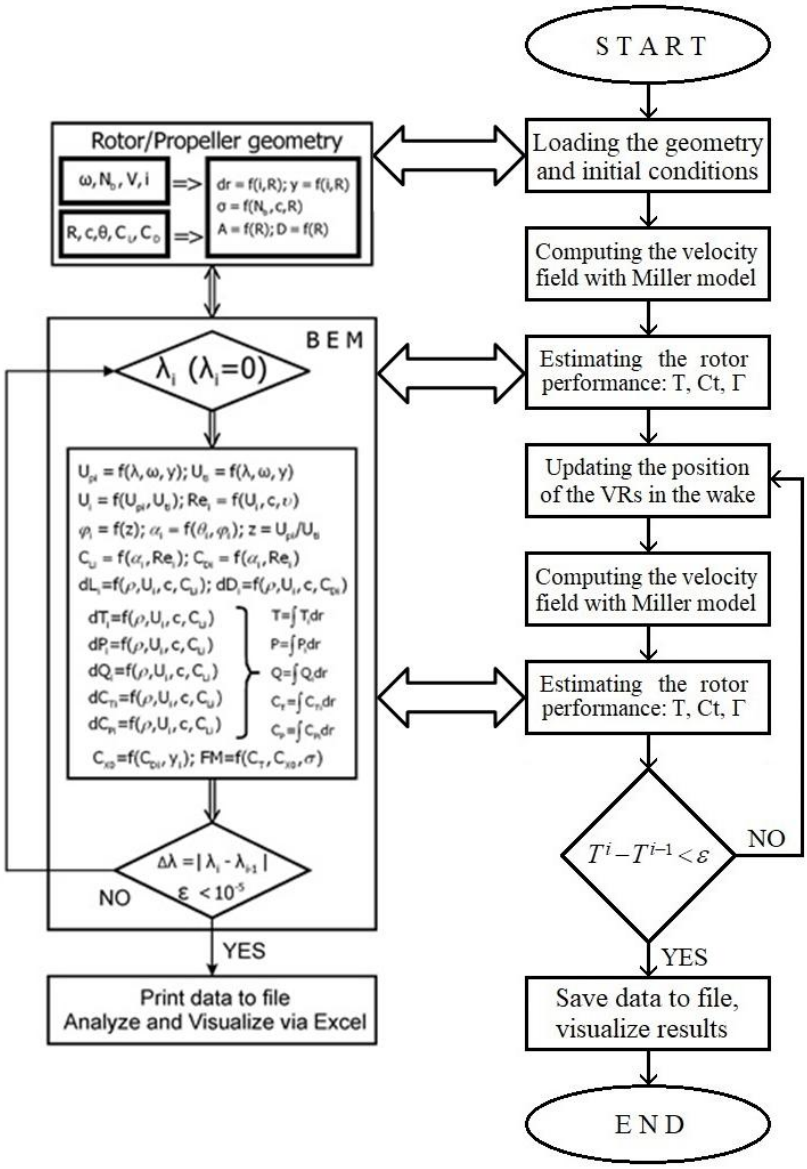

FIG. 2. Algorithm of the coupled BEM-vortex model.

By keeping constant the values of both the angular velocity of the rotor Ω and the pitch angle of the blades θ, the numerical model is evaluating the rotor parameters in hover flight. However, the presented program module is also capable of studying the rotor performance in smooth transition from one operational regime to another, as well as for an abrupt step-change of the pitch angle of the blades θ.

For this present study assumed is a stable hover, which is a hover performed in zero wind conditions. The results from this study are presented in section 5 "Results from the numerical study".

The model rotor, which is used as reference geometry in those studies, has two rectangular untwisted blades of NACA0012 profile. The tip radius R of the blades is 288mm, the root radius at the hub mounting r_0 is 65mm and the chord length c is 25mm. The pitch angle of the blades θ is adjustable and thus can be varied between wind tunnel experiments.

Shown on Fig. 3 is the velocity triangle in a typical cross-section of the blade. The velocity of the axial flow through the plane of rotation, resulting from the work of the rotor, is denoted with V_z.

In the literature it is referred as the axial induced velocity and is a function of the operational parameters of the rotor, namely the angular velocity Ω and the pitch angle of the blade θ. The speed of rotation of the section in the plane of the rotor is denoted with $U = \Omega y$, where y is the blade station radius, which varies from r_0 to R. For the tip of the blade $y = R$ and $U = \Omega R = V_{tip}$. The relative air speed for the cross-section of the blade W is computed with (1):

$$W = \sqrt{U^2 + V_z^2} \,. \tag{1}$$

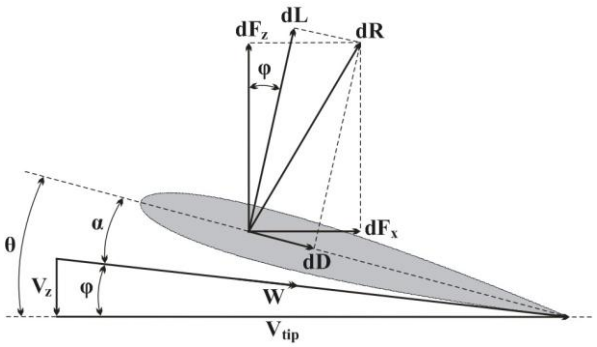

FIG. 3. Triangle of velocities in the cross-section of the rotor

3.1 Numerical approach

According to [11], by assuming uniform bound circulation and a single tip-trailing vortex per blade, the vortex strength can be computed with:

$$\Gamma = \frac{2T}{\rho N_b R V_{tip}} \,, \tag{2}$$

where T is the total thrust produced by the model rotor at a fixed angular velocity Ω and pitch angle of the blades θ. R is the tip radius of the blades, $V_{tip} = \Omega R$ is the velocity at the tip of the blades, N_b is the number of blades of the rotor and ρ is the density of the air.

For every change in either the angular velocity Ω or the pitch angle of the blades θ, the total thrust of the rotor T and the bound circulation Γ are also changed. Equation (2) is used for the computation of the bound circulation Γ.

In [1] the coefficient of thrust C_T is defined as:

$$C_T = \frac{T}{\rho A \Omega^2 R^2} \,, \tag{3}$$

where T is the total thrust produced by the rotor; ρ is the density of the air; Ω is the angular velocity of the rotor; R is the radius of the rotor and $A = \pi R^2$ is the area of the rotor disc. Equation (4) is used for the computation of the coefficient of thrust C_T.

From Fig. 2 it can be observed that for an increase of the axial induced velocity V_z there is a decrease of the angle of attack α. The smaller is the angle of attack of the cross-sectional airfoil, the smaller is the local thrust increment ΔF_z. Thus the total thrust of the rotor T reduces and with it reduces the coefficient of thrust C_T.

On Fig. 4 are shown the key dimensions, used in the computation of the induced velocity in a point of the flow-field. The dimensions y_m, y_n, z_m and z_n are universal for both the cylindrical and contracting wake models. Those are the coordinates of two points, namely M and N. It is considered that the induction happens in point M by a vortex element, situated at point N.

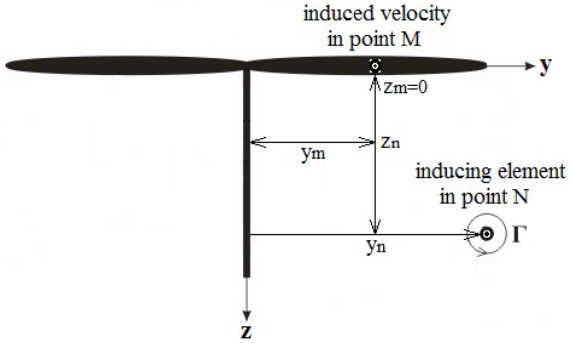

FIG. 4. Dimensions used in the computation of the induced velocity field of the rotor

Lewis [13] introduces the dimensionless parameters *y* and *z* with (4) and (5):

$$z = \frac{z_m - z_n}{y_n}, \tag{4}$$

$$y = \frac{y_m}{y_n}. \tag{5}$$

Those are used for the derivation of the equations for the axial V_z and radial V_y induced velocities. For the case of the semi-infinite vortex cylinder, the axial velocity is computed with (6) and for the case of $y = 1$, (7) is used:

$$V_{z,cyl} = \frac{\Gamma}{4\pi}\left\{B + \frac{z}{\sqrt{z^2 + (y+1)^2}}\left[K\left(k^2\right) - \frac{y-1}{y+1}\Pi\left(n,k^2\right)\right]\right\}, \tag{6}$$

$$V_{z,cyl_{(y=1)}} = \Gamma\left(\frac{1}{4} + \frac{z\,K\left(k^2\right)}{2\pi\sqrt{z^2+4}}\right). \tag{7}$$

For the case of a semi-infinite vortex cylinder, the radial induced velocity is computed with (8):

$$V_{y,cyl} = \frac{2\Gamma}{\pi k^2\sqrt{z^2 + (y+1)^2}}\left[E\left(k^2\right) - \left(1 - \frac{k^2}{2}\right)K\left(k^2\right)\right]. \tag{8}$$

The constant *B* in (6) depends from the ratio between the outer radius of the vortex cylinder and the radius of the rotor. For the case of $y = 1$ it is:

$$\mathrm{B}_{(y=1)} = \frac{\pi}{2}. \tag{9}$$

For the case of the system of vortex rings, the axial induced velocity is computed with (10) and for the radial induced velocity (11) is used:

$$V_{z,ring} = \frac{\Gamma}{2\pi y_n\sqrt{z^2 + (y+1)^2}}\left\{K\left(k^2\right) - \left[1 + \frac{2(y-1)}{z^2 + (y-1)^2}\right]E\left(k^2\right)\right\}, \tag{10}$$

$$V_{y,ring} = \frac{\Gamma z}{2\pi y y_n \sqrt{z^2 + (y+1)^2}} \left\{ K\left(k^2\right) - \left[1 + \frac{2y}{z^2 + (y-1)^2} \right] E\left(k^2\right) \right\}. \quad (11)$$

Equations (6), (7), (8), (10) and (11) contain complete elliptic integrals of the first $E(k^2)$, second $K(k^2)$ and third kind $\Pi(n,k^2)$. The elliptic parameters n and k are introduced with (12) and (13).

$$k = \sqrt{\frac{4y}{z^2 + (y+1)^2}}, \quad (12)$$

$$n = \frac{4y}{(y+1)^2}. \quad (13)$$

Equations (14) and (15) are used for the application of second-order Adams-Bashforth predictor:

$$y_i^P = y_i^n + \frac{\Delta t}{2}\left[3V_{iy}\left(y_i^n, z_i^n\right) - V_{iy}\left(y_i^{n-1}, z_i^{n-1}\right) \right]. \quad (14)$$

$$z_i^P = z_i^n + \frac{\Delta t}{2}\left[3V_{iz}\left(y_i^n, z_i^n\right) - V_{iz}\left(y_i^{n-1}, z_i^{n-1}\right) \right]. \quad (15)$$

Equations (16) and (17) are used in the corrector step.

$$y_i^{n+1} = y_i^n + \frac{\Delta t}{2}\left[V_{iy}\left(y_i^P, z_i^P\right) + V_{iy}\left(y_i^n, z_i^n\right) \right], \quad (16)$$

$$z_i^{n+1} = z_i^n + \frac{\Delta t}{2}\left[V_{iz}\left(y_i^P, z_i^P\right) + V_{iz}\left(y_i^n, z_i^n\right) \right], \quad (17)$$

The model updates the coordinates y and z with an Adams-Bashforth predictor step, followed by a corrector step. It is referred as the Adams-Bashforth predictor-corrector scheme of second order.

Numerical instability issues are observed if the vortex rings in the near wake are not being initially slightly contracted. Thus, a simple arrangement with linear contraction higher than 10% is found to be enough to assure stable computation.

4. RESULTS AND DISCUSSIONS

On Fig. 5 are shown three computational cases for the flow-field of the rotor in hover, computed with the Miller model for a rotor configuration with four blades and five emitted vortex rings per blade. The numerical computations are performed for 2000 RPM and θ=10deg for three different values of the parameter d_1, namely 0.25p for case a); 0.5p for case b) and 0.75p for case c), where p is the average spacing between the vortex rings in the near wake. In all three cases d_0 is set to 0.1p.

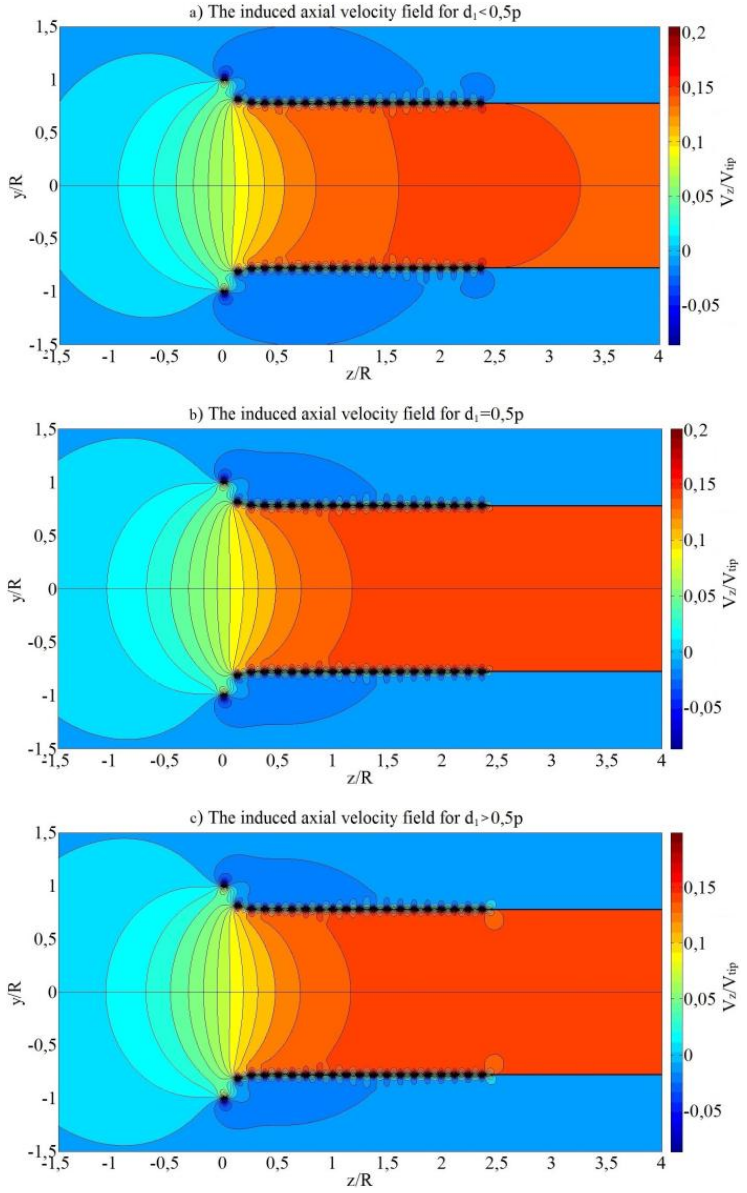

FIG. 5. The flow-field of the rotor for 2000 RPM and θ=10deg, computed with the BEM-vortex model with the second-order predictor-corrector scheme.

From the numerical results for the flow-field, presented on Fig. 5, it becomes apparent that the optimal value for the placement of the semi-infinite vortex cylinder behind the last vortex ring d_1, is the same as the average spacing of the vortex rings in the near wake d_1=0.5p. This is due to the fact that the most uniform velocity field is formed for this spacing and also it is the only setting, for which the average computed value of the axial induced velocity V_z in the plane of the rotor z/R = 0 double its value in the far wake beyond z/R = 4, such as predicted by the theory for a rotor in hover.

In Table 1 are compared the coefficient of thrust C_T, the percentage error $|\Delta|$ and the required computational time t_{comp} for the simulations performed with a rotor configuration with four blades, where two, three or five vortex rings are emitted per blade. The spacing parameters for all computations are set as follows: d_0=0.1p and d_1=0.5p.

Table 1. Comparison of the results obtained for four blade rotor configuration for two, three, five and ten vortex rings per blade against the wind tunnel experiment data

Models	***4 blade rotor 2 VRs per blade***	***4 blade rotor 3 VRs per blade***	***4 blade rotor 5 VRs per blade***	***4 blade rotor 10 VRs per blade***	***4 blade rotor experiment***
C_T $[10^{-3}]$	2.939	2.861	2.684	2.742	2.569
$\|\Delta\|$ [%]	14.4	11.4	4.47	6.73	-
t_{comp} [s]	0.19	0.23	0.37	0.63	-

From the results presented in Table 1, it can be seen that initially the percentage error decreases with the increase of the number of the emitted vortex rings per blade being taken into account for the modelling of the near wake. However, the additional increase of the number of emitted vortex rings per blade, is not only increasing the required computational time t_{comp} but it is also increasing the percentage error.

CONCLUSION

The presented approach for the numerical simulation of the performance of a rotor in hover, showed good computational stability and adequate accuracy of the obtained results, when compared with the experimental data. Although the added complexity from the integration of a time-stepping predictor-corrector scheme, the coupled BEM-vortex model retains its computational rapidity, which can be explained with good convergence of the numerical solution.

In order to obtain adequate rotor performance estimation figures with the presented numerical approach, it is recommended to use between 5 and 10 emitted vortex rings per blade, regardless of the rotor configuration.

The existing percentage error between the computational results and the experimental data is acceptable. Therefore, the proposed model can be used for preliminary studies and simulations of the expected thrust and overall performance of newly designed rotors.

FUTURE WORK

The results from the conducted study, presented in this paper, encourage the authors to use the coupled BEM-vortex model with time-stepping predictor-corrector scheme, in order to study the thrust of small rotors in unsteady operational condition. The intent is to perform a series of studies on the rotor performance during transient operational regimes, produced by both big and small rates of change in the angular velocity of the rotor Ω; and for both positive and negative rates of change.

Of special interest is to study the changes in the thrust, resulting from a rapid change of the pitch angle of the blades θ for a constant angular velocity of the rotor Ω. Such a study will provide greater insights into the rotor performance during the transition period, in which the flow-field is adjusting to the new operating conditions of the rotor.

REFERENCES

[1] J. G. Leishman, Principles of Helicopter Aerodynamics, 1st ed., New York: Cambridge University Press, 2000, pp. 43-44;

[2] M. Ramasamy, T. E. Lee and J. G. Leishman, "Flow-field of a Rotating-Wing Micro Air Vehicle", Journal of Aircraft, Vol. 44, 2007;

[3] K. J. Hayman and K. R. Reddy, "Calculation of the velocity field generated by a helicopter main and tail rotors in hover", ARL-AERO-TM-366, Aerodynamics Research Laboratories, Australia, 1984;
[4] R. H. Miller, "Simplified Free Wake Analysis for Rotors", FFA TN 1982-07, Sweden, 1982;
[5] F. Panayotov, I. Dobrev, F. Massouh and M. Todorov, "Numerical model for rapid computation of the flow-field of a rotor in hover", ICMT-2017, pp. 570-577, DOI: 10.1109/MILTECHS.2017.7988822, Czech Republic, 2017;
[6] A. J. Landgrebe, "An analytical method for predicting rotor wake geometry", Journal of the American Helicopter Society, Vol. 14, No. 4, October 1969, pp. 20-32;
[7] A. J. Landgrebe, "An analytical and experimental investigation of helicopter rotor hover performance and wake geometry characteristics", US Army Air Mobility Research and Development Laboratory, Technical Report 71-14, USA, 1971;
[8] R. H. Miller, "Rotor hovering performance using the method of fast free wake analysis", Journal of Aircrafts, vol. 20, 1983;
[9] A. Bagai and J. G. Leishman, "Adaptive grid sequencing and interpolation schemes for helicopter rotor wake analyses", AIAA Journal, Vol. 36, No. 9, September 1998, pp.1593-1602;
[10] F. Panayotov, I. Dobrev, F. Massouh and M. Todorov, "Studying the wake contraction of the flow-field of a rotor in hover", BulTrans-2017, DOI: 10.1051/matecconf/201713301009, Bulgaria, 2017;
[11] A. Karpatne, J. Sirohi, S. Mula and C. Tinney, "Vortex ring model of tip vortex aperiodicity in a hovering helicopter rotor", Journal of Fluids Engineering, ASME, vol. 136, 2014;
[12] R. H. Miller, T. W. Roberts and E. M. Murman, "Computational methods for wake modelling and blade airload determination in hover and forward flight", Computers and Mathematics with Applications, vol. 12A, 1986;
[13] R. I. Lewis, Vortex Element Methods for Fluid Dynamic Analysis of Engineering Systems, New York: Cambridge University Press, 1991, pp. 147-170.